Available online at www.sciencedirect.com
SCIENCE DIRECT®
Journal of Solid State Chemistry 177 (2004) 4126–4135
JOURNAL OF SOLID STATE CHEMISTRY
www.elsevier.com/locate/jssc

An experimental investigation of ionic transport properties in $CuI–Ag_2WO_4$ and $CuI–Ag_2CrO_4$ mixed systems

S. Austin Suthanthiraraj*, Y. Daniel Premchand

Department of Energy, University of Madras, Guindy Campus, Chennai 600 025, India

Received 16 May 2004; received in revised form 27 July 2004; accepted 31 July 2004
Available online 7 October 2004

Abstract

The phenomenon of ionic transport in the case of two different mixed systems $(CuI)_{(1-x)}–(Ag_2WO_4)_x(0.15\leqslant x\leqslant 0.6)$ and $(CuI)_{(1-y)}–(Ag_2CrO_4)_y(0.15\leqslant y\leqslant 0.5)$ has been investigated. Powder X-ray diffraction (XRD) analysis coupled with differential scanning calorimetry (DSC), Fourier transform infrared (FT-IR), FT-Raman and electrical transport studies involving ionic transport number and temperature-dependent electrical conductivity measurements have been carried out in order to identify the various phases responsible for the conduction process. The occurrence of typical ionic conductivity values of $4.5\times10^{-3}\,Scm^{-1}$ for the composition $(CuI)_{0.45}–(Ag_2WO_4)_{0.55}$ and $1.1\times10^{-4}\,Scm^{-1}$ in the case of $(CuI)_{0.55}–(Ag_2CrO_4)_{0.45}$ at room temperature has been discussed in terms of the observed characteristics.

Keywords: Electrical conductivity; Ionic conduction; Solid-state reaction

1. Introduction

Fast ion conducting materials have attracted the interest of many researchers in recent years because of their potential application as electrolytes in solid-state batteries, sensors, electrochemical displays and so on [1]. A number of such ion conducting systems have been identified over the years and their electrical properties investigated widely. More recently, development of a new solid electrolyte system involving CuI and silver oxyacid salt Ag_2MoO_4 was attempted by us through a systematic study of ion transport, electrical and electrochemical properties [2,3]. It was demonstrated through these studies that the effective electrical conduction in several compositions of such systems may be correlated to the constituent phases and their structural features as well. Stimulated by this success, we have now extended our investigation to two different pseudobinary mixed systems namely, $CuI–Ag_2WO_4$ and $CuI–Ag_2CrO_4$ through X-ray diffraction (XRD), differential scanning calorimetry (DSC), Fourier transform infrared (FT-IR) and electrical conductivity studies. The results thus obtained have been discussed in the light of the relationship between ionic conduction and phases identified.

2. Experimental

Powder specimens of the solid systems $(CuI)_{(1-x)}–(Ag_2WO_4)_x(0.15\leqslant x\leqslant 0.6)$ and $(CuI)_{(1-y)}–(Ag_2CrO_4)_y$ $(0.15\leqslant y\leqslant 0.5)$ were prepared from analar grade cuprous iodide (CuI) and the respective silver oxyacid salt by melt quenching method. Desired amounts of the starting materials namely, CuI and Ag_2WO_4 in the case of $(CuI)_{(1-x)}–(Ag_2WO_4)_x$, were annealed in Pyrex glass tubes at 823 K for 330 min before being quenched in liquid nitrogen. On the other hand, the specimens of $(CuI)_{(1-y)}–(Ag_2CrO_4)_y$ system were obtained by annealing cuprous iodide (CuI) and Ag_2CrO_4 together at 873 K in Pyrex glass tubes for 330 min and quenching the same

*Corresponding author. Fax: +91-44-235-2494.
E-mail address: suthan98@yahoo.com (S.A. Suthanthiraraj).

0022-4596/$ - see front matter © 2004 Elsevier Inc. All rights reserved.
doi:10.1016/j.jssc.2004.07.053

into liquid nitrogen. Silver tungstate (Ag_2WO_4) and Silver chromate (Ag_2CrO_4) used for the preparation were initially precipitated from aqueous solutions of $AgNO_3$ and analar Na_2WO_4 or Na_2CrO_4 under safe-light conditions.

The XRD patterns for each of the prepared samples were obtained using a Siefert X-ray diffractometer with Cu$K\alpha_1$ radiation ($\lambda = 1.541$ Å). Differential scanning calorimetric (DSC) experiments were carried out on a Perkin Elmer Model DSC-7 calorimeter over the temperature range 323–623 K at a heating rate of 20°/min under nitrogen atmosphere. The FT-IR absorption spectra in the 400–1000 cm^{-1} range were recorded for the specimens on a Burger IFS66 V FT-IR spectrometer, by the KBr pellet method. FT-Raman spectrum for the typical sample having $x = 0.45$ in the $(CuI)_{(1-y)}$–$(Ag_2CrO_4)_y$ system, was obtained on a Burger IFS66V FT-IR-Raman spectrometer with a 1064 nm excitation of YAG laser at 200 mW. The impedance measurements were made on pellet samples of 8 mm diameter sandwiched between a pair of metallic silver disc electrodes using a Hewlett Packard (model HP 4284A) Precision LCR meter in the frequency range 20 Hz–1 MHz from room temperature to 445 K. For the estimation of ionic transport number t_i, open circuit voltage (OCV) values of galvanic cells fabricated with the configuration (−) Ag/Sample/I_2 (+) were measured and compared with the theoretical value of 687 mV [4,5].

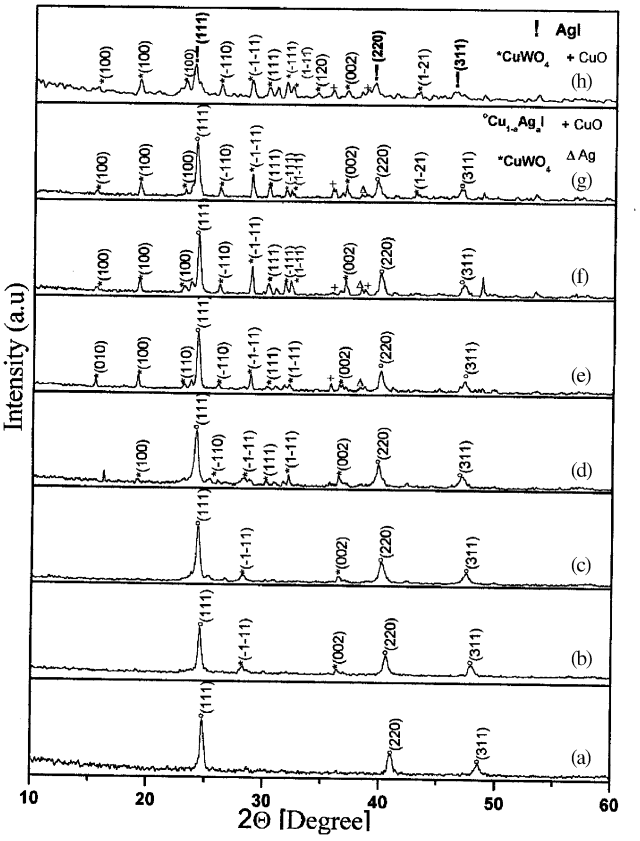

Fig. 1. Powder XRD patterns obtained for various compositions in the $(CuI)_{(1-x)}$–$(Ag_2WO_4)_x$ system: (a) $x = 0.15$; (b) $x = 0.2$; (c) $x = 0.25$; (d) $x = 0.3$; (e) $x = 0.35$; (f) $x = 0.4$; (g) $x = 0.45$ and (h) $x = 0.5$.

3. Results and discussion

3.1. Phase identification

3.1.1. $(CuI)_{(1-x)}$–$(Ag_2WO_4)_x$ System ($0.15 \leqslant x \leqslant 0.6$)

3.1.1.1. XRD and DSC data. The room temperature XRD patterns obtained during the present investigation for eight different compositions containing $x = 0.15$, 0.2, 0.25, 0.3, 0.35, 0.4, 0.45 and 0.5 in the pseudobinary mixed system $(CuI)_{(1-x)}$–$(Ag_2WO_4)_x$ are shown in Fig. 1. All the XRD patterns presented in Fig. 1 are found to show well-defined diffraction lines corresponding to various phases in the rapidly quenched $(CuI)_{(1-x)}$–$(Ag_2WO_4)_x$ mixture, whereas similar XRD patterns obtained in the case of $x = 0.55$ sample (not shown) were rather broad and free from any strong and definite diffraction lines thereby indicating its amorphous-like nature. The detection and identification of reflection lines in the XRD patterns have been carried out through the XRD analysis software XRDA aided by JCPDS-International Center for Diffraction Data. On the other hand, the XRD pattern obtained for $x = 0.6$ appeared to contain only few feable peaks (not shown).

The analysis of individual XRD patterns representing different compositions in Fig. 1, appears to indicate the presence of a set of three prominent diffraction lines (marked °), which are consistent with the γ-phase of CuI [6], while being indexed as (111), (220) and (311) on the basis of the face centered cubic unit cell of the space group $F\bar{4}3m$. These reflection lines with peak values at $2\Theta = 24.794°$, 40.998° and 48.516° in the XRD pattern for the typical composition with $x = 0.15$, have their peak values shifted towards lower 2Θ values in the case of higher x value patterns. Subsequently, their peak values of $2\Theta = 23.705°$, 39.185° and 46.232° for $x = 0.5$ (marked !) are found to match those for γ-AgI [7]. The lattice parameter values of 6.222, 6.288, 6.355, 6.41, 6.393, 6.42, 6.442 and 6.496 Å estimated on the basis of their X-ray line positions analyzed using the standard software XRDA tend to suggest the formation of solid solutions of the type $Ag_aCu_{1-a}I$ ($0 < a < 1$) between ionic salts such as AgI and CuI. Further, an interesting aspect of these solid solutions is that they exist over an entire concentration range [8,9] and their lattice parameters vary according to Vegard's law [10]. The fact that the relationship between concentration and lattice parameter of $Ag_aCu_{1-a}I$ obeys Vegard's law, give us the liberty to derive the stoichiometry of any hypothetical member of the (Ag,Cu)I family of solid solution directly from their lattice parameter values as explained elaborately in our previous paper [2]. Accordingly, the

individual members of solid solutions in the case of $x = 0.15$, 0.2, 0.25, 0.3, 0.35, 0.4 and 0.45 are identified to be $Cu_{0.63}Ag_{0.37}I$, $Cu_{0.48}Ag_{0.52}I$, $Cu_{0.32}Ag_{0.68}I$, $Cu_{0.2}Ag_{0.8}I$, $Cu_{0.24}Ag_{0.76}I$, $Cu_{0.17}Ag_{0.83}I$ and $Cu_{0.12}Ag_{0.88}I$, respectively. In view of the fact that the present work concerns with a qualitative analysis of various phases, the authors did not contemplate chemical analysis of individual compositions, though it would have provided more information.

On the other hand, the set of diffraction lines (marked *), noticed in all these patterns appear to indicate the presence of $CuWO_4$ (triclinic, space group $P\bar{1}$), in the range $0.15 \leqslant x \leqslant 0.5$ [11,12]. However, there are some challenges involved in the identification of reflection lines from other minor phases like CuO (marked +) and Cu_2WO_4. The reflections from these minor phases may be either weak or overlapping with reflections from the $CuWO_4$ phase. This concerns the reflection lines of CuO, (111) and (−111) at $2\Theta = 38.75^\circ$ and 35. 56° as they overlap with the (200) and (0−21) reflections of $CuWO_4$, respectively, in the XRD patterns of $x = 0.3$, 0.35, 0.4, 0.45 and 0.5. Similarly, the (020) reflection corresponding to $CuWO_4$ seems to overlap with the possible (2−21) reflection lines of Cu_2WO_4. However, the absence of the next intense line corresponding to (−102) and (300) in the X-ray patterns is indicative of the fact that the reflection line at $2\Theta = 30.806^\circ$ may not be the one associated with Cu_2WO_4. Further a particular line that appears at $2\Theta = 38.2^\circ$, in the case of Figs. 1(e), (f) and (g), may be due to the presence of metallic silver (marked △) in the case of samples having $x = 0.35$, 0.4 and 0.45.

One of the most interesting features of these XRD results is the identification of solid solutions of the type $Ag_aCu_{1-a}I$, formed due to the solid-state reaction occurring between the starting materials namely, CuI and Ag_2WO_4 during the melting process. The structure of this particular mixed system $Ag_aCu_{1-a}I$ has been widely studied and it is known that $Ag_aCu_{1-a}I$ ($0.5 \leqslant a \leqslant 1$) undergoes a phase transition to α-form (anions form a bcc structure) over the temperature range 420–550 K [13], whereas $Ag_aCu_{1-a}I$ ($0 < a < 0.5$) in the temperature between 550 and 660 K changes into probable α-form (anions form fcc crystal structure) [14]. On the other hand, the phase diagram of the (Cu,Ag)I system was reported by Nolting [15]. However, the other major phase in the chosen system namely $CuWO_4$ having triclinic structure space group $P\bar{1}$, is not known to undergo any phase change at high temperatures [16].

Fig. 2 depicts the DSC thermograms recorded for the various compositions having $x = 0.15$, 0.2, 0.25, 0.3, 0.45, 0.5, 0.55 and 0.6 in the mixed system $(CuI)_{(1-x)}$–$(Ag_2WO_4)_x$. The endothermic peaks that appear at 593, 560, 541, 470 and 459 K in the case of DSC plots for $x = 0.15$, 0.2, 0.25, 0.3 and 0.45

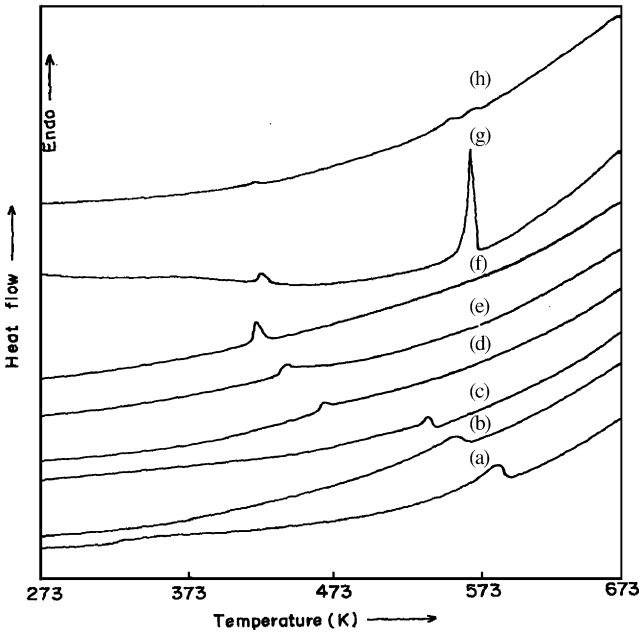

Fig. 2. DSC thermograms recorded for the samples in $(CuI)_{(1-x)}$–$(Ag_2WO_4)_x$ system: (a) $x = 0.15$; (b) $x = 0.2$; (c) $x = 0.25$; (d) $x = 0.3$; (e) $x = 0.45$; (f) $x = 0.5$; (g) $x = 0.55$ and (h) $x = 0.6$.

compositions are found to agree with the $\gamma \rightarrow \alpha$ phase transition temperature of $Ag_aCu_{1-a}I$ solid solution indicated by Nolting [15]. These thermal features appear to indicate that the solid solutions in the composition range $x = 0.15-0.45$ follow their compositions estimated from XRD, while the appearance of an endothermic peak at 421 K in the case of the particular sample having $x = 0.5$, may be attributed to the $\gamma \rightarrow \alpha$ phase transition temperature of AgI [17]. Similarly, the occurrence of an endothermic peak at 424 K in the case of $x = 0.6$ compositions is an indication of the presence of γ-AgI as one of their constituent phases. On the other hand, the endothermic peak that appears at 569 K in the case of $x = 0.55$ composition is found to compare well with the observed melting temperature of AgI–Ag_2WO_4 glasses [18–20]. It reveals the presence of Ag_2WO_4, that could be treated as Ag_2WO_4 (excess) [2], once the limit of the solid-state reaction between CuI and Ag_2WO_4 has been achieved with $x = 0.45$ composition.

3.1.1.2. FT-IR analysis. Fig. 3 depicts the FT-IR spectra obtained for $x = 0.5$, 0.55 and 0.6 compositions in the $(CuI)_{(1-x)}$–$(Ag_2WO_4)_x$ system though the expected bands for the solid solutions $Ag_aCu_{1-a}I$ fall in the Far-IR region. It is interesting to note from Fig. 3 that the vibration bands observed at 895, 749, 613, 558 and 464 cm^{-1} in the case of $x = 0.5$ agree well with that of crystalline $CuWO_4$ [21]. In fact, the presence of $CuWO_4$ in the sample having $x = 0.5$ has already been confirmed by the XRD studies as well. Similarly, in the FT-IR spectra for $x = 0.55$ and 0.6 compositions, those

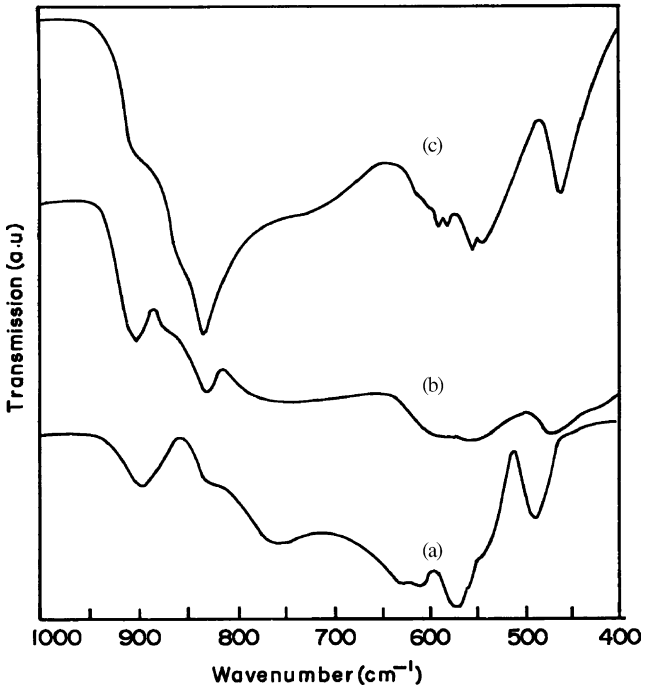

Fig. 3. FT-IR spectra observed for the specimens: (a) $x = 0.5$; (b) $x = 0.55$ and (c) $x = 0.6$ in the $(CuI)_{(1-x)}$–$(Ag_2WO_4)_x$ system.

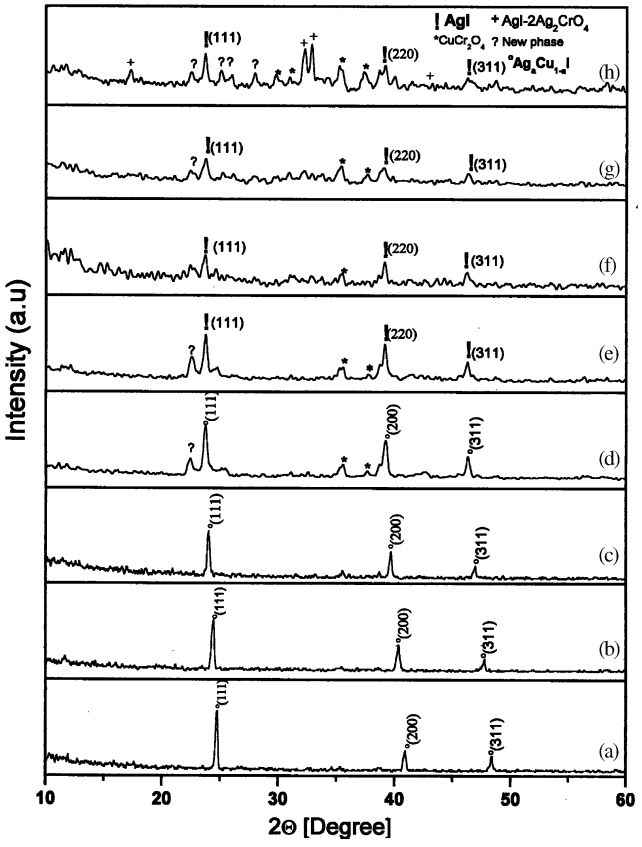

Fig. 4. Powder XRD patterns obtained for various compositions in the $(CuI)_{(1-y)}$–$(Ag_2CrO_4)_y$ system: (a) $y = 0.15$; (b) $y = 0.2$; (c) $y = 0.25$; (d) $y = 0.3$; (e) $y = 0.33$; (f) $y = 0.4$; (g) $y = 0.45$ and (h) $y = 0.5$.

bands observed at 902, 742 and 469 cm^{-1} may be attributed to the $CuWO_4$ phase [21], while the presence of a new band at 827 cm^{-1} is comparable to the vibration band at 830 cm^{-1} noticed in AgI–Ag_2WO_4 glasses [18]. Therefore, it is reasonable to assume that both $x = 0.55$ and 0.6 samples possess octahedral WO_6 units of Ag_2WO_4 designated as Ag_2WO_4 (excess) as well. Interestingly, the structure of $CuWO_4$ as revealed by XRD studies is considerably different from that of Ag_2WO_4 (crystal) containing octahedral WO_6 units [22,23]. Since, the tungsten atom in $CuWO_4$ is located within a slightly distorted octahedron, it is considerably displaced from the center [12]. Therefore, in the light of these facts, it is reasonable to assume that the oxyanion structure in these samples consists mostly of WO_6 units.

3.1.2. $(CuI)_{(1-y)}$–$(Ag_2CrO_4)_y$ system ($0.15 \leqslant y \leqslant 0.5$)

3.1.2.1. XRD and DSC results. Fig. 4 depicts the room temperature powder XRD patterns obtained for eight different samples in the mixed system $(CuI)_{(1-y)}$–$(Ag_2CrO_4)_y$ where $y = 0.15$, 0.2, 0.25, 0.3, 0.33, 0.4, 0.45 and 0.5, respectively. In the XRD patterns presented in Fig. 4, those lines indexed as (111), (220) and (311), correspond to the reflections from $Ag_aCu_{1-a}I$ ($0 < a < 1$) solid solution (marked °) or AgI (marked !), identified on the basis of Zinc blende structures of γ-CuI and γ-AgI; fcc unit cell with 'a' values 6.06 and 6.496 Å, respectively. As in the case of $(CuI)_{(1-x)}$–$(Ag_2WO_4)_x$ system, the calculated lattice parameter values of 6.24, 6.32, 6.42 and 6.46 Å, reveal the individual solid solutions in the rapidly quenched samples of $y = 0.15$, 0.2, 0.25 and 0.3 compositions as $Cu_{0.59}Ag_{0.41}I$, $Cu_{0.4}Ag_{0.6}I$, $Cu_{0.17}Ag_{0.83}I$, and $Cu_{0.06}Ag_{0.94}I$, respectively, whereas the appearance of those peaks at $2\Theta = 23.72$, 39.12 and 46.23° in Figs. 2(d)–(g) indicates the presence of γ-AgI in $y = 0.33$, 0.4, 0.45 and 0.5 compositions. The presence of AgI in these compositions is indicative of the fact that the solid-state reaction between CuI and Ag_2CrO_4 has proceeded until the solid solution of the type $Cu_{1-a}Ag_aI$ is complete, which is further confirmed by the features of DSC plots shown in Fig. 5. The occurrence of endothermic peaks ascribable to the $\gamma \rightarrow \alpha$ phase transition of AgI at 420 K in the DSC plots of $y = 0.33-0.5$ compositions tends to notify the presence of AgI, whereas the set of endothermic peaks that occur at 579, 547, 458 and 426 K in the case of $y = 0.15$, 0.2, 0.25 and 0.3 compositions are comparable to the transition temperatures of $Ag_aCu_{1-a}I$ solid solutions present within these samples.

A careful analysis of the XRD patterns in Fig. 4 also reveals the formation of various other phases apart from $Ag_aCu_{1-a}I$ solid solution or AgI. The onset of formation can be witnessed from the observed lines corresponding to $CuCr_2O_4$ (marked *) and new phase

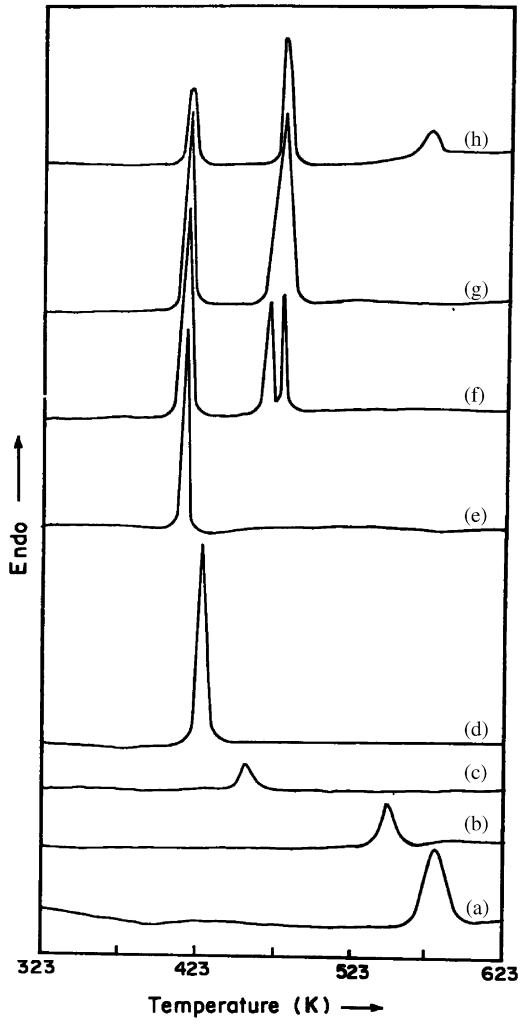

Fig. 5. DSC thermograms recorded for the samples in $(CuI)_{(1-y)}$–$(Ag_2CrO_4)_y$ system: (a) $y = 0.15$; (b) $y = 0.2$; (c) $y = 0.25$; (d) $y = 0.3$; (e) $y = 0.33$; (f) $y = 0.4$; (g) $y = 0.45$ and (h) $y = 0.5$.

(marked ?), in the XRD patterns of $y = 0.25-0.5$ composition range. Interestingly, peaks noticed at $2\Theta = 32.83°$, $32.22°$, $37.24°$ and $39.97°$, in the XRD patterns for $y = 0.5$ (marked +), composition is found to match exactly with those peaks observed for an intermediate compound AgI–$2Ag_2CrO_4$ and reported in the phase diagram studies of AgI–Ag_2CrO_4 glasses [19]. In fact, the formation of AgI–Ag_2CrO_4 phase in the case of $y > 0.33$ compositions is a reality as the amount of Ag_2CrO_4 in excess of the limiting composition has led to the presence of Ag_2CrO_4 (excess) in the reaction melt once the solid-state reaction between CuI and Ag_2CrO_4 is over. Further evidence into this argument may be due to the additional endothermic peaks observed in the DSC plots of these compositions apart from those corresponding to AgI. The endothermic peak at 479 K in the DSC plots for those samples having $y = 0.4$ and 0.45 and that at 478 K in the case of $y = 0.5$ as shown in Fig. 5 are similar to the endothermic peak observed in the case of AgI–Ag_2CrO_4 glasses having higher concentration of AgI (67–100 mol% AgI) which is at least 5–10 K below 488 K, the eutectic point observed in the case of AgI–Ag_2CrO_4 glasses having 78 mol% AgI [19]. The appearance of an additional endothermic peak at 569 K apart from the set of endothermic peaks at 420 and 478 K in the case of $y = 0.5$ may be associated with the melting of AgI–Ag_2CrO_4 phase in the mixture, as is evident from the phase diagram for AgI–Ag_2CrO_4 glasses [19]. Therefore, the DSC results have indicated the unambiguous presence of AgI–Ag_2CrO_4 (excess) phase in the samples having $y = 0.4$, 0.45 and 0.5 apart from AgI, $CuCr_2O_4$ and other minor phases identified by XRD results.

3.1.2.2. FT-IR and FT-Raman results. Fig. 6 displays the FT-IR spectra obtained for those samples having $y = 0.4$, 0.45 and 0.5, in the mixed system $(CuI)_{(1-y)}$–$(Ag_2CrO_4)_y$. The observed FT-IR spectra of these samples show a strong absorption band at 879 cm^{-1} and a shoulder at about 851 cm^{-1}, which may be, respectively, assigned to the v_3 and v_1 modes of vibration of tetrahedral CrO_4^{2-} ions [21]. Hence, it is apparent that CrO_4^{2-} ions constitute the anionic species in the range $y = 0.4-0.5$. Furthermore, Fig. 7 presents the FT-Raman spectrum obtained for the typical composition $y = 0.45$. The FT-Raman spectrum observed in the range 100–1200 cm^{-1} has been resolved into three Lorentzian peaks at 352, 465 and 815 cm^{-1}, respectively. The most intense peak, which appears at about 815 cm^{-1}, in the spectrum, may be compared with the Raman peak observed at 811 cm^{-1} due to Cr (IV)–O stretching, in the case of solid Ag_2CrO_4 [24] whereas,

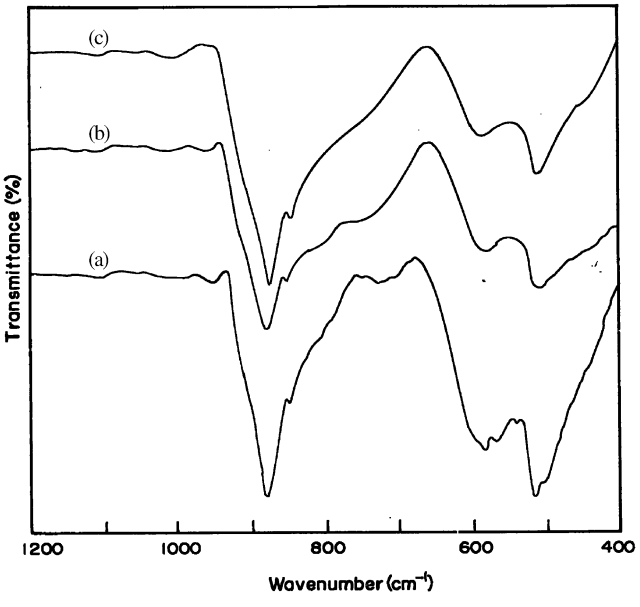

Fig. 6. FT-IR spectra observed for the specimens: (a) $y = 0.4$; (b) $y = 0.45$ and (c) $y = 0.5$ in the $(CuI)_{(1-y)}$–$(Ag_2CrO_4)_y$ system.

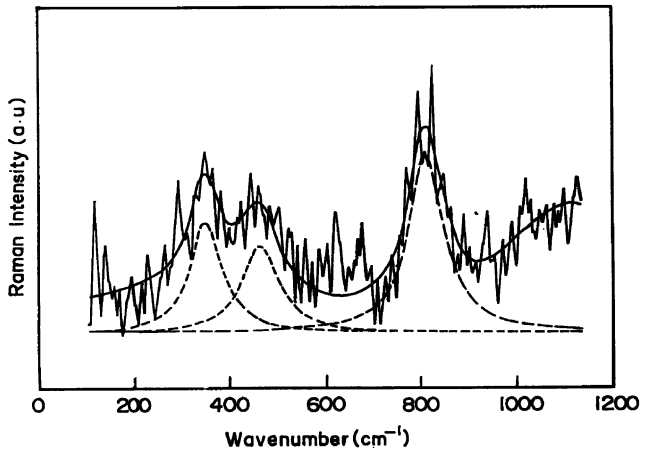

Fig. 7. FT-Raman spectra observed for the typical composition $(CuI)_{0.55}$–$(Ag_2CrO_4)_{0.45}$ in the $(CuI)_{(1-y)}$–$(Ag_2CrO_4)_y$ system.

those Raman peaks at 352 and 465 cm^{-1} may be assigned to the v_2 and v_4 modes of vibration in CrO_4^{2-} anions [25].

3.2. Electrical conductivity results

3.2.1. $(CuI)_{(1-x)}$–$(Ag_2WO_4)_x$ system ($0.15 \leqslant x \leqslant 0.6$)

Fig. 8 depicts the complex impedance plots obtained at different temperatures for $x = 0.2$ composition in the $(CuI)_{(1-x)}$–$(Ag_2WO_4)_x$ system. It may be observed from Fig. 8 that the impedance plot at room temperature (293 K) is a well-defined semicircle as the intersection of low frequency end of the semicircle with the Z'-axis pertaining to the bulk was used to determine the effective electrical conductivity (σ). On the other hand, the high temperature impedance plots are found to show the presence of a low frequency arc, which arises due to the effect of electrode polarization and is incomplete in the frequency range, studied. The value of bulk conductivity at these temperatures was estimated from the intersection point of the high frequency semicircles on the real axis. It is also interesting to note from these plots that the intersection point corresponding to bulk impedance tends to shift towards lower and lower Z' values with increase in temperature indicating that ion diffusion is thermally activated.

The effective electrical conductivity values for various compositions in the $(CuI)_{(1-x)}$–$(Ag_2WO_4)_x$ system are shown in Fig. 9 as a function of reciprocal of absolute temperature. A careful examination of Fig. 9 reveals that among the set of $\log \sigma T$ vs. $1000/T$ plots shown for various compositions, those plots corresponding to the compositions $x = 0.5$ and 0.6 are found to indicate an abnormal increase in conductivity at around 420 K. This behavior of conductivity with temperature corresponds to the transition of silver iodide from β to α phase, as in the case of AgI–Ag_2WO_4 [20]. However, the conductivity increase in these compositions appears to be more gradual than an abrupt increase noticed in the case of AgI–Ag_2WO_4 glasses, perhaps due to the presence of $CuWO_4$ and CuO in the reaction mixture. On the other hand, the variation of $\log \sigma T$ with $1000/T$ for all the other compositions is found to be linear with a negative slope, suggesting an Arrhenius type of behavior for conductivity (σ), over the temperature range 293–420 K,

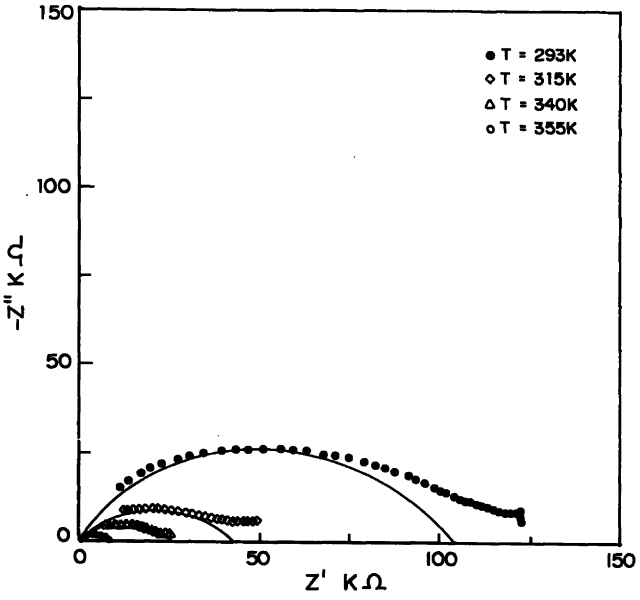

Fig. 8. Complex impedance plots obtained for the typical composition having $x = 0.2$ in the system $(CuI)_{(1-x)}$–$(Ag_2WO_4)_x$ at different temperatures.

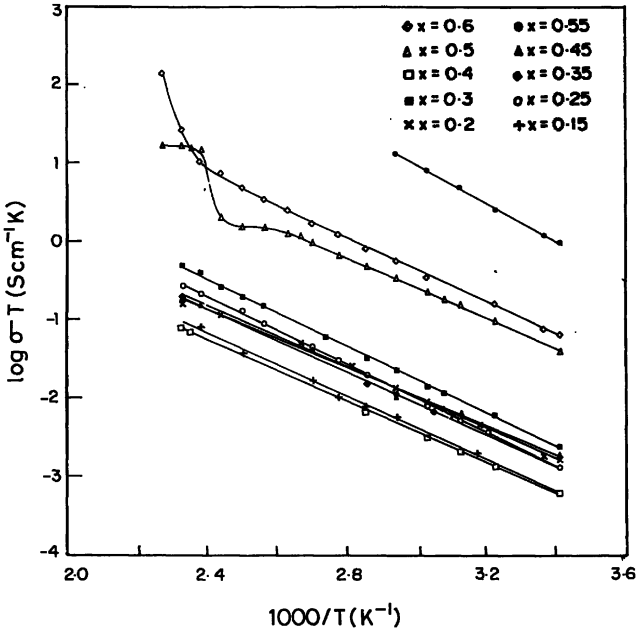

Fig. 9. Temperature dependence of conductivity for various samples in the $(CuI)_{(1-x)}$–$(Ag_2WO_4)_x$ ($0.15 \leqslant x \leqslant 0.6$) system.

except in the case of a typical composition with $x = 0.55$, where the electrical conductivity values are not consistent beyond 350 K. The apparent (effective) activation energy values for the effective electric conduction in the above compositions have been evaluated from the slopes of the best-fit lines obtained for their respective Arrhenius plots.

Table 1 presents the room temperature conductivity ($\sigma_{293\,K}$) values for various compositions in the $(CuI)_{(1-x)}$–$(Ag_2WO_4)_x$ system along with their activation energy values for effective conduction and the ionic transport number data (t_i) evaluated at 293 K by EMF technique. It is obvious from Table 1 that the best conducting composition namely, $(CuI)_{0.45}$–$(Ag_2WO_4)_{0.55}$, which contains an amorphous framework exhibits an effective electrical conductivity value of $4.5 \times 10^{-3}\,Scm^{-1}$ at room temperature (293 K), while two other compositions $x = 0.5$ and 0.6 are found to possess effective electrical conductivity values of 1.3×10^{-4} and $2.6 \times 10^{-4}\,Scm^{-1}$, respectively. The fact that these compositions posses a large transport number value of 0.99 at room temperature (293 K) and effective electrical conductivity values of the order of 10^{-4}–$10^{-3}\,Scm^{-1}$ appears to reveal the feasibility of obtaining appreciably high silver ion conduction as in the case of similar pseudobinary mixed system, AgI–Ag_2WO_4 [18,20] which may be explained further on the basis of the constituent phases in these samples. Obviously, the observed conductivity data for $x = 0.55$ is much larger than $x = 0.5$ and 0.6 and comparable to that of well-known silver ion conducting AgI–Ag_2WO_4 solid electrolyte system. During the present investigation, the occurrence of an electrical conductivity of the order of $10^{-3}\,Scm^{-1}$ at room temperature for $x = 0.55$ may be reasonably attributed to the presence of AgI dispersed in an amorphous framework as revealed by the XRD results. Furthermore, the abnormal variation in conduction noticed in the remaining compositions may be correlated satisfactorily to the presence of constituent phases such as $CuWO_4$ and CuO but the relative content of these phases has not been ascertained quantitatively.

Table 1
Results of electrical transport studies for various compositions in the mixed system $(CuI)_{(1-x)}$–$(Ag_2WO_4)_x$ $(0.15 \leqslant x \leqslant 0.6)$

Composition x	Room temperature conductivity $\sigma_{293\,K}$ Scm^{-1}	Activation energy E_a (eV)	Ionic transport number t_i
0.15	2×10^{-6}	0.41	0.53
0.2	6.2×10^{-6}	0.41	0.74
0.25	4.3×10^{-6}	0.42	0.79
0.3	8.3×10^{-6}	0.42	0.85
0.35	4.1×10^{-6}	0.40	0.81
0.4	2.1×10^{-6}	0.39	0.84
0.45	6.9×10^{-6}	0.37	0.87
0.5	1.3×10^{-4}	0.36	0.99
0.55	4.5×10^{-3}	0.36	0.99
0.6	2.6×10^{-4}	0.39	0.99

Copper (I) iodide is a solid electrolyte with Cu^+ fast ion conduction in the high temperature α and β phases, where as the low temperature zinc blende type CuI is found to exhibit ionic conductivity only of the order of $10^{-7}\,Scm^{-1}$ [26,27]. In the present study, CuI in the γ form has been allowed to react with Ag_2WO_4 having an electrical conductivity in the order of $10^{-9}\,Scm^{-1}$ [20], at high temperature and an attempt made to freeze their reaction product by quenching them to liquid nitrogen temperature. Based on the XRD and DSC studies these phases are identified to be $Ag_aCu_{1-a}I$ solid solution, $CuWO_4$ and CuO in the case of samples having $x = 0.15$, 0.2, 0.25, 0.3, 0.35, 0.4 and 0.45, whereas AgI happens to be the halide phase formed due to the solid-state reaction between CuI and Ag_2WO_4 in the $x = 0.5$ composition. As is well known, AgI has three different modifications. Under ordinary temperature and pressure, it crystallizes in Zinc blende type (γ-AgI) and wurzite type (β-AgI), and at 420 K it transforms to the high temperature phase (α-AgI), which has a bcc structure [28]. α-AgI is a fast ionic conductor with silver ions as the mobile species and its electrical conductivity of $1 \times 10^{\circ}\,Scm^{-1}$ at 423 K, is 10^4 or 10^6 times larger than that of γ or β phase [29]. The activation energies of conduction for γ- and β-AgI at near room temperature are about 0.31 and 0.41 eV, respectively [30]. On the other hand, $CuWO_4$, which is the other major phase in the mixture, is a known electronic conductor with an electrical conductivity of $9.26 \times 10^{-12}\,Scm^{-1}$ at 301 K [16].

Silver iodide is also known to form high conducting solid electrolytes with many complex salt systems. The silver iodide–oxyacid salt combinations, for example, are mostly high conductive with considerably less activation energy whereas their ionic transference numbers are almost unity [31]. In particular, AgI–Ag_2WO_4 glasses investigated by many researchers including $Ag_6I_4WO_4$ solid electrolyte synthesized by Takahashi et al. [20] were found to have ambient temperature electrical conductivities as large as $10^{-2}\,Scm^{-1}$ and very low activation energies around 0.16 eV, at ambient conditions. Similar highly conducting solid electrolytes prepared by the authors within the pseudobinary system of CuI–Ag_2MoO_4 by rapid quenching were found to contain mixtures of AgI, Ag_2MoO_4 (excess) and Cu_2MoO_4 phases and the role of these oxysalts in conduction phenomenon has also been successfully discussed in detail [3,4]. However, the preparatory condition of the present $(CuI)_{(1-x)}$–$(Ag_2WO_4)_x$ system is such that the availability of oxygen for the oxidation of copper cannot be ruled out. As a consequence, Cu_2WO_4 would probably have transformed in the

presence of air into $CuWO_4$ and CuO [32], whereas, the presence of AgI and Ag_2WO_4 phases within the solid $(CuI)_{0.45}$–$(Ag_2WO_4)_{0.55}$ is already evident from the DSC results. Further, the observed room temperature electrical conductivity value of $4.5 \times 10^{-3}\,Scm^{-1}$ is found to be at least three orders of magnitude higher than the typical conductivity value $10^{-6}\,Scm^{-1}$ observed for γ-AgI and on a par that of AgI–Ag_2WO_4 glasses. Therefore, it is reasonable to attribute the observed effective electrical conductivity of the $x = 0.55$ composition in the $(CuI)_{(1-x)}$–$(Ag_2WO_4)_x$ system to the presence of AgI dispersed in a an amorphous framework.

It is also worthwhile to mention that room temperature electrical conductivity values only of the order of $10^{-6}\,Scm^{-1}$, could be observed in the case of $x = 0.15$, 0.2, 0.25, 0.3, 0.35, 0.4 and 0.45 compositions having $Ag_aCu_{1-a}I$ solid solution as the constituent halide phase. Studies on ion conducting $Ag_aCu_{1-a}I$ $(0<a<1)$ solid solutions in γ-phase carried out earlier in our laboratory have suggested effective electrical conductivity values of the order of 10^{-6}–$10^{-5}\,Scm^{-1}$ for these solid solutions and activation energies for ionic migration in 0.43–0.54 eV range [33]. These observations are found to be in good agreement with the results of temperature-dependent conductivity measurements made by Brightwell et al. [34]. Further, those solid solutions in the higher side of AgI were reported to behave like pure silver ion conductors with unit transport number by Schmidt and Bazan [35] whereas their total electrical conductivity values were much lower than AgI but higher than that for CuI. The observed effective electrical conductivity values of those samples in the $x = 0.15-0.45$ range are comparable to the effective electrical conductivity values of $Ag_aCu_{1-a}I$ solid solutions and their apparent (effective) activation energy values of 0.41, 0.41, 0.42, 0.42, 0.40, 0.39, 0.37 indicate a similar conductivity process at low temperatures. These transport features strongly suggest that $Ag_aCu_{1-a}I$ solid solutions formed due to the solid-state reaction between CuI and Ag_2WO_4, may have a major role in the effective electric conduction of these compositions in the mixed system.

Interestingly, during the measurement of 't_i' by the EMF technique involving silver anode solid-state cells of the type (−) Ag/Sample/I_2 (+), it was reported that Cu^+ ions do not contribute any potential to the measured EMF owing to their lower oxidation potential as compared to that of Ag^+ ions [36]. Hence, it is reasonable to argue that the measured t_i values would not contain any contribution from Cu^+ ions. Accordingly, t_i values of 0.53, 0.74, 0.79, 0.85, 0.81, 0.84 and 0.87 noticed in the case of $x = 0.15$, 0.2, 0.25, 0.3, 0.35, 0.4 and 0.45 indicate that the remaining contribution to the total conductivity may be due to other ionic species namely, Cu^+ ions and electronic conduction in view of the fact that the above samples are identified to be a mixture of $Ag_aCu_{1-a}I$ $(0 \leqslant a \leqslant 1)$ solid solution and $CuWO_4$ by the present XRD, DSC and FT-IR studies.

3.2.2. $(CuI)_{(1-y)}$–$(Ag_2CrO_4)_y$ system $(0.15 \leqslant y \leqslant 0.5)$

Fig. 10 shows the plots of $\log \sigma T$ obtained as a function of $(1000/T)$ for the eight typical compositions in the $(CuI)_{(1-y)}$–$(Ag_2CrO_4)_y$ $(0.15 \leqslant y \leqslant 0.5)$ system over the temperature range 295–445 K. It is observed from Fig. 10 that the conductivity plots representing $y = 0.3$, 0.33, 0.4, 0.45 and 0.5 compositions show an abnormal increase in conductivity above 420 K. This sudden change in the behavior of $y = 0.33$, 0.4, 0.45 and 0.5 compositions may be compared to the typical endothermic transitions noticed at 421, 422, 421 and 421 K corresponding to the $\beta \rightarrow \alpha$ phase transition temperature of AgI noticed in the DSC thermograms. Similarly, the observed increase in conductivity at around 425 K in the plot of $\log \sigma T$ vs. $1000/T$ for the $y = 0.3$ composition agrees quite well with the phase transition witnessed in the isothermal conductivity plots of $Ag_{0.94}Cu_{0.06}I$ solid solutions [33] and comparable to the endothermic peak observed at 426 K in the DSC curves. On the other hand, the conductivity curves for those compositions in the $y = 0.15-0.3$ range show no abrupt change phase transition up to 445 K. The observed straight-line behavior of these plots of $\log \sigma T$ vs. $1000/T$ is indicative of the fact that such compositions exhibit Arrhenius-type of conductivity variation.

The apparent (effective) activation energy values for ionic migration calculated from these plots have been listed in Table 2 along with the effective electrical conductivity values at room temperature ($\sigma_{295\,K}$) and

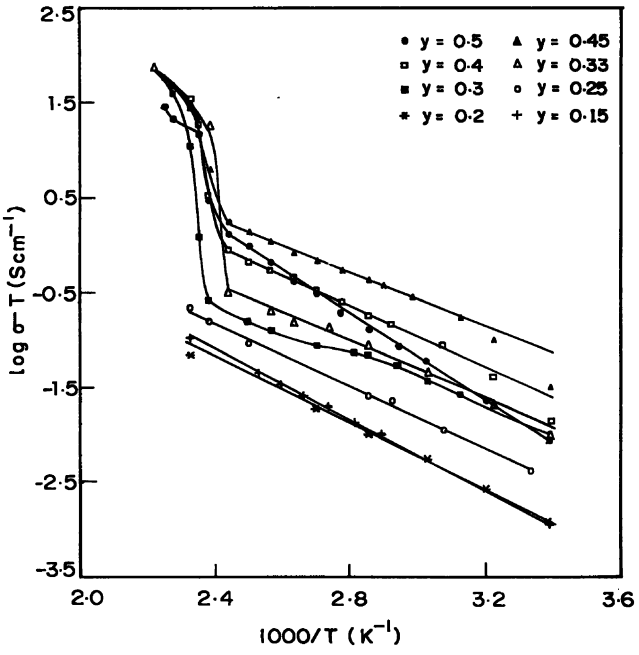

Fig. 10. Temperature dependence of conductivity for various samples in the $(CuI)_{(1-y)}$–$(Ag_2CrO_4)_y$ $(0.15 \leqslant y \leqslant 0.5)$ system.

Table 2
Results of electrical transport studies for various compositions in the mixed system $(CuI)_{(1-y)}$–$(Ag_2CrO_4)_y$ $(0.15 \leqslant y \leqslant 0.5)$

Composition y	Room temperature conductivity $\sigma_{293\,K}$ Scm^{-1}	Activation energy E_a (eV)	Ionic transport number t_i
0.15	3.7×10^{-6}	0.37	0.45
0.2	4.0×10^{-6}	0.35	0.81
0.25	5.4×10^{-6}	0.33	0.94
0.3	2.9×10^{-5}	0.33	0.97
0.33	3×10^{-5}	0.33	0.99
0.4	2.1×10^{-6}	0.32	0.99
0.45	1.1×10^{-4}	0.29	0.99
0.5	2.9×10^{-5}	0.4	0.99

ionic transport number data (t_i) evaluated by EMF technique at 295 K. It can be seen from Table 2 that compositions of $y = 0.15$, 0.2, 0.25 and 0.3 posses effective electrical conductivity (σ_{295}) values quite comparable with that of $Ag_aCu_{1-a}I$ solid solutions. The transport number 't_i' values estimated by EMF technique indicate that both Ag^+ and Cu^+ ions are active and their activation energies calculated from the $\log \sigma T$ vs. $1000/T$ plots lie in the 0.37–0.33 eV region. The XRD and DSC results have indicated these compositions as a mixture of $Ag_aCu_{1-a}I$ solid solution and other minor phases including $CuCr_2O_4$. Under isolated conditions, the ambient temperature (electronic) conductivity of spinel structured $CuCr_2O_4$ is practically negligible when compared with the observed electrical conductivity values of $Ag_aCu_{1-a}I$ solid solutions. Accordingly, it is obvious that the $Ag_aCu_{1-a}I$ solid solution has a major role in the effective electrical conductivity of these specimens.

On the other hand, the XRD and DSC results have revealed the formation of AgI due to solid state reaction between CuI and Ag_2CrO_4 in the case of $x = 0.33$, 0.4, 0.45 and 0.5 compositions, whereas the presence of Ag_2CrO_4 (excess) is confirmed by the thermal analysis and spectral studies. In view of these revelations, the influence of AgI and Ag_2CrO_4 phases on the transport properties of these compositions may be analyzed in the light of the arguments dealing with $(CuI)_{(1-x)}$–$(Ag_2WO_4)_x$ system in the preceding section. These compositions have an ambient temperature ionic transport number 't_i' value of 0.99 and their activation energy calculated from the Arrhenius relationship is found to be the lowest for the highest conducting composition $y = 0.45$. In other words, an appreciably high electrical conductivity of $1.1 \times 10^{-4}\,Scm^{-1}$ has been realized in the case of the sample with $y = 0.45$ that possesses the lowest activation energy value of 0.29 eV. This effective electrical conductivity value is at least two orders of magnitude higher than that for γ-AgI and may be attributed to AgI and Ag_2CrO_4 (excess) phase, the presence of which is evident from the results of the XRD and DSC studies.

4. Conclusions

The present investigation on $(CuI)_{(1-x)}$–$(Ag_2WO_4)_x$ $(0.15 \leqslant x \leqslant 0.6)$ and $(CuI)_{(1-y)}$–$(Ag_2CrO_4)_y$ $(0.15 \leqslant y \leqslant 0.5)$ solid electrolyte systems has indicated their multi-phase nature. The occurrence of the best ionic conduction in the composition $(CuI)_{0.45}$–$(Ag_2WO_4)_{0.55}$ is due to the presence of AgI dispersed in an amorphous framework. Similarly, the best conducting composition in the latter system namely, $(CuI)_{0.55}$–$(Ag_2CrO_4)_{0.45}$ has been attributed to the formation of AgI.

References

[1] R.M. Dell, Solid State Ionics 134 (2000) 139–158.
[2] S.A. Suthanthiraraj, Y.D. Premchand, J. Solid State Chem. 170 (2003) 142–153.
[3] S.A. Suthanthiraraj, Y.D. Premchand, Ionics 9 (2003) 301–307.
[4] K. Kiukkola, C. Wagner, J. Electrochem. Soc. 104 (1957) 379–387.
[5] J.S. McKechni, L.D.S. Turner, C.A. Vincent, J. Chem. Thermodyn. 11 (1979) 1189–1195.
[6] JCPDS File no: 06-0246.
[7] JCPDS File no: 78-0641.
[8] M. Kusakabe, Y. Shirakawa, S. Tamaki, Y. Ito, J. Phys. Soc. Japan 64 (1995) 170–176.
[9] J. Bosko, J. Rybicki, Solid State Ionics 157 (2003) 227–232.
[10] T. Takahashi, N. Wakabayashi, O. Yamamoto, J. Solid State Chem. 21 (1977) 73–78.
[11] JCPDS File no: 21-0307.
[12] L. Kihlborg, E. Gebert, Acta Crystallogr. B 26 (1970) 1020–1026.
[13] K. Endo, T. Ida, J. Kimura, M. Mizuno, M. Suhura, K. Kihara, Chem. Phys. Lett. 308 (1999) 390–396.
[14] J. Kimura, T. Ida, M. Mizuno, K. Endo, M. Suhura, K. Kihara, J. Mol. Struct. 522 (2000) 61–69.
[15] J. Nolting, Ber. Bunsenges Phys. Chem. 68 (1964) 932–939.
[16] S.K. Arora, T. Mathew, N.M. Batra, J. Cryst. Growth 88 (1988) 379–382.
[17] M. Tatsumisago, K. Okuda, N. Itakura, T. Minami, Solid State Ionics 121 (1999) 193–200.
[18] M. Hosono, J. Kawamura, H. Itoigawa, N. Kuwata, T. Kamiyama, Y. Nakamura, J. Non-Cryst. Solids 244 (1999) 81–88.
[19] A. Magistris, G. Chiodelli, G.V. Campari, Z. Naturforsch. 31a (1976) 974–977.
[20] T. Takahashi, S. Ikeda, O. Yamamoto, J. Electrochem. Soc. 120 (1973) 647–651.
[21] G.M. Clark, W.P. Doyle, Spectrochim. Acta 22 (1966) 1441–1447.
[22] P.M. Skarstad, S. Geller, Mater. Res. Bull. 10 (1975) 791–799.
[23] A. Turkovic, D.L. Fox, J.F. Scott, S. Geller, G.F. Ruse, Mater. Res. Bull. 12 (1977) 189–195.
[24] B.I. Hurley, R.L. McCreery, J. Electrochem. Soc. 150 (2003) 367–373.
[25] H. Stammreich, D. Bassi, O. Sala, Spectrochim. Acta 12 (1958) 403–405.
[26] S. Villain, J. Cabane, D. Roux, L. Roussel, P. Knauth, Solid State Ionics 76 (1995) 229–235.
[27] J.X.M.Z. Johansson, I. Ebbsjo, R.L. McGreevy, Solid State Ionics 82 (1995) 115–122.

[28] J.C. Philips, J. Electrochem. Soc. 123 (1976) 934–940.
[29] T. Ida, K. Kimura, Solid State Ionics 107 (1998) 313–318.
[30] J.R.G. Patnaik, C.S. Sunandana, J. Phys. Chem. Solids 59 (1998) 1059–1069.
[31] M.D. Ingram, A.H.J. Robertson, Solid State Ionics 94 (1997) 49–54.
[32] F.A. Gimelfarb, A.N. Zelikman, Tsvetnaya Metall. 10 (1963) 63–66.
[33] N. Chellamal, N. Gogulamurali, S.A. Suthanthiraraj, P. Maruthamuthu, Bull. Electrochem. 6 (1990) 625–626.
[34] J.W. Brightwell, C.N. Buckley, B. Ray, Solid State Ionics 15 (1985) 331–333.
[35] J.A. Schmidt, R. Fornari, J.C. Bazan, Electrochim. Acta 24 (1979) 1131–1132.
[36] S. Murugesan, S.A. Suthanthiraraj, P. Maruthamuthu, Solid State Ionics 154–155 (2002) 621–628.